Polymer 50 (2009) 3974–3980

Contents lists available at ScienceDirect

Polymer

journal homepage: www.elsevier.com/locate/polymer

Preparation of photochromic poly(vinylidene fluoride-*co*-hexafluoropropylene) fibers by electrospinning

Mao Wang [a], Sean A. Vail [b], Amy E. Keirstead [b,c], Manuel Marquez [d,e,f], Devens Gust [b], Antonio A. Garcia [d,*]

[a] *Center for Research and Technology, Philip Morris USA, Richmond, VA 23219, USA*
[b] *Department of Chemistry and Biochemistry, Arizona State University, Tempe, AZ 85287, USA*
[c] *Department of Chemistry and Physics, University of New England, Biddeford, ME 04005, USA*
[d] *Harrington Department of Bioengineering, Arizona State University, Tempe, AZ 85287, USA*
[e] *Center for Integrated Nanotechnologies, Los Alamos National Laboratory, Los Alamos, NM 87545, USA*
[f] *YNANO LLC, Midlothian, VA 23113, USA*

ARTICLE INFO

Article history:
Received 19 February 2009
Received in revised form
12 June 2009
Accepted 20 June 2009
Available online 26 June 2009

Keywords:
Electrospinning
Photochromic fibers

ABSTRACT

Photochromic poly(vinylidene fluoride-*co*-hexafluoropropylene) (PVDF-*co*-HFP) fibers were prepared by electrospinning from a solution of copolymer and ester-functionalized nitrospiropyran (SPEST) molecules. The surface and internal features of the electrospun (ES) fibers were characterized by scanning electron microscopy (SEM), Fourier transform infrared spectroscopy (FTIR) and wide-angle X-ray diffraction (WAXD). The strong segregation of fluorine-rich groups on the fiber surface, which occurs during and/or after the electrospinning process, is driven by the lower surface tension for fluorine-rich groups and leads to encapsulation of SPEST predominantly near the core of the fibers, as confirmed by both X-ray photoelectron spectroscopy (XPS) and dynamic water contact angle (CA) measurements. The photochromic behavior of the spiropyran is preserved in the polymeric fibers, as confirmed by steady-state absorption and emission spectroscopy. Both isomeric forms of the photochrome in SP-PVDF-*co*-HFP were emissive, an effect that is thought to be due to the steric and/or electrostatic restrictions on the ring-opening reaction imposed by the fiber.

1. Introduction

Electrospinning (ES) is a convenient method for synthesizing continuous polymeric fibers with diameters ranging from a few nanometers to several hundred nanometers [1–3]. Nonwoven mats of ES fibers have been investigated for potential applications such as filtration and immobilization membranes [4–7], drug-delivery agents [8–11], biosensors [12–16], scaffoldings for tissue engineering [17,18] and composites for the fabrication of protective clothing [19,20]. Contemporary electrospinning techniques have been developed that align fibers with specific orientations and manipulate fiber architecture [21–28]. Recent interest in combining top-down electrospinning technology with bottom-up molecular self-assembly has resulted in the production of novel nanostructures that would otherwise not be possible. For example, in the case of poly(methyl methacrylate-*co*-tetrahydroperfluorooctyl acrylate) ES fibers, most of the fluorocarbon species segregate onto the fiber surface due to low surface tension [29]. Polydimethylsiloxane (PDMS) blocks also tends to migrate to the surface of poly(styrene-*block*-dimethylsiloxane) ES fibers, which, in combination with the inherent roughness of ES fiber mats, has led to the development of fabrics that exhibit superhydrophobic properties [30]. Rutledge et al. and Joo et al. independently reported a co-electrospinning technique for constructing unique morphologies consisting of alternating stacked disks or concentric cylinders within continuous ES poly(styrene-*block*-polyisoprene) fibers by annealing at different temperatures [31–33]. On the other hand, the incorporation of various moieties including nanoparticles, proteins or other small species into ES (homopolymer) fibers has afforded polymeric materials that exhibit such properties as magnetism, conductivity or biocompatibility [34–45]. Certainly, it would prove beneficial to effectively utilize molecular self-assembly to direct the spatial distribution of various species within ES fibers.

Photochromism is the light-induced reversible interconversion between isomeric species exhibiting distinct optical absorption characteristics. Spiropyrans have long been recognized as an attractive class of photochromic molecules since they typically undergo rapid, efficient and reversible changes in optical absorption arising from photoinduced isomerizations following

* Corresponding author. Tel.: +1 480 965 8798; fax: +1 480 727 7624.
E-mail address: tony.garcia@asu.edu (A.A. Garcia).

0032-3861/$ – see front matter © 2009 Elsevier Ltd. All rights reserved.
doi:10.1016/j.polymer.2009.06.044

irradiation with alternating doses of ultraviolet (UV) and visible (vis) light. The significant changes in molecular conformation and dipole that accompany spiropyran photoisomerization have been used as a means to photomodulate peptide structure and/or function [46,47] and cell adhesion [48,49] as well as to develop photochromism-based protein assays [50]. As illustrated in Fig. 1, spiropyrans exist as a nonpolar (closed) *spiro* form (SP) in the dark in nonpolar environments, or when exposed to visible light [51, 52]. The SP form is virtually colorless and absorbs primarily in the region below 400 nm. Irradiation with UV light (<400 nm) affords a vividly colored and highly polar (open) *merocyanine* form (MC) that exhibits characteristically strong absorption in the region between 450 and 600 nm. The photoinduced switching between MC and SP forms can be preserved for thousands of cycles in some cases under anaerobic conditions.

A number of recent studies describe the preparation of spiropyran-modified surfaces [53–57], nanoparticles [58,59], membranes [60,61], nanopores [62,63] and colloids [64–66]. Encapsulation of spiropyrans within a continuous, polymeric, nanofibrous matrix could confer certain advantages. First, the state of the photochrome could be modulated via the unidirectional alignment of the SP along the nanofibers, thereby allowing for selective irradiation of the SP along the fibrous "wire"; in this way, the directionality of the photochromic fibers could be controlled. Second, due to the small diameters, the SP-containing nanofibrous membranes have large surface areas, which could increase the sensitivity and reduce the time necessary for SP to respond to the irradiation. In addition, a polymeric nanofiber matrix could provide mechanical support and minimize chemical, radiative and corrosive degradation. The degree of reversibility or rate of change in color intensity could also be controlled by selecting an appropriate fiber matrix. Photochromic fibers could find wide applications in areas such as optical sensors, optical gates, optical data storage devices and processing media.

Herein, we report the preparation of hydrophobic PVDF-*co*-HFP ES fibers containing nitrospiropyran molecules functionalized with a 1′-(3-carbomethoxypropyl) side-chain (SPEST). The photochromic microfibers (SP-PVDF-*co*-HFP) were electrospun from a solution of PVDF-*co*-HFP in *N,N*-dimethylacetamide (DMAc) and acetone containing 1 wt% SPEST. PVDF-*co*-HFP was selected because of its abundance of hydrophobic fluorine side chains, excellent thermal stability, considerable resistance to corrosion, chemical and UV degradation, and appreciable mechanical durability. Due to low surface tension, the vast majority of fluorine-rich groups are expected to migrate onto the fiber surface during and after the electrospinning process, which could protect the SPEST from adverse environmental effects within (or near) the core of the fibers.

2. Experimental details

All reagents were purchased from Sigma–Aldrich and used without further purification. 1′-(3-carbomethoxypropyl)-3′,3'-dimethyl-6-nitrospiro-[2H-1]benzopyran-2,2′-indoline (SPEST) was prepared as previously described [66].

2.1. Electrospinning

Due to the relatively high boiling point of DMAc, wet ES fibers were obtained from PVDF-*co*-HFP when DMAc was used neat. To circumvent this, acetone was added in order to increase the solvent evaporation rates during electrospinning. The optimal solvent ratio in terms of electrospinnability and dryness of the fibers was found to be 3:2 DMAc:acetone. PVDF-*co*-HFP (10, 12 and 15 wt%) solution was prepared by dissolution of the polymer in the DMAc–acetone mixed solvent system. The spiropyran (SPEST, 1 wt% with respect to PVDF-*co*-HFP) was added into this solution prior to electrospinning. The solution was electrospun onto aluminum foil using a point-to-plate assembly. The electrical potential (7 kV), solution flow rate (0.9 mL/h) and capillary tip to collector plate distance (25 cm) were adjusted for stable electrospinning. The same parameters were used for electrospinning of SP-PVDF-*co*-HFP fibers.

2.2. Characterization

SEM images were obtained using an FEI XL30 environmental scanning electron microscope (ESEM) operating at 15 kV in hi-vac mode. The ES fibers were sputter coated with 15 nm of Au–Pd to facilitate high resolution imaging. A Cressington 208HR sputter coater operating under an argon atmosphere was used to coat the samples with Au–Pd. The samples were mounted onto 12 mm diameter carbon adhesive disks that were attached to A1 stubs. The WAXD measurements were performed on a Rigaku D-MAX with half-degree optics over a range of 2θ from 10 degrees to 60 degrees with an angular step of 0.02 degrees. The scattering from the polymer is relatively weak, and thus to eliminate any scattering from other materials the samples were mounted on a quartz zero-background holder. The X-ray source was Cu Kα with a wavelength of 1.54059 Å. Infrared spectra were measured with a Bruker Equinox 55 FTIR spectrometer. Each spectrum was acquired in transmission mode by accumulation of 256 scans with a resolution of 4 cm^{-1}. XPS on ES fibers was performed with a Kratos XSAM800 equipped with an ion-pumped sample analysis chamber and a turbo-pumped sample introduction chamber. Secondary electrons are analyzed via a hemispherical electron energy spectrometer that feeds an electron multiplier/phosphor-screen/reticon-tube detection center. Secondary electron excitation is obtained via a dual-anode (Al/Mg) X-ray gun. Surface analysis was performed on the fiber samples (1 cm × 1 cm) using circular regions (diameter approximately 1–2 cm) located towards the center of the sample with Al Kα radiation operating at 3 E^{-10} Torr. The detection limit for this method is 5 nm below the surface. Contact angle measurements were carried out as previously described [67] with the following differences. Rectangular samples of PVDF-*co*-HFP and SP-PVDF-*co*-HFP fibers were separately adhered to glass microscope slides. In the case of the SPEST-modified fiber, the sample was irradiated with UV ($\lambda = 365$ nm, 10 min) or visible ($\lambda > 520$ nm, 10 min) light just prior to measurements. Due to inherent surface roughness, five sequential CA measurements were taken on the same spot in order to minimize variations due to significant differences in surface

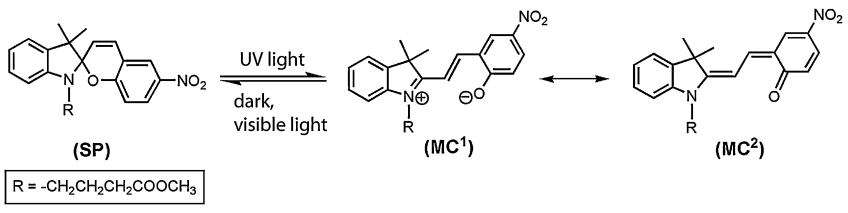

Fig. 1. Photoisomerization pathways for SPEST (SP and MC forms) following exposure to UV or visible light.

morphologies in the sample; the reported value is the average of the five measurements.

2.3. Steady-state absorption and emission spectroscopy

Ultraviolet–visible (UV–vis) ground-state absorption spectra were measured on a Shimadzu UV3101PC UV–Vis–NIR spectrophotometer. Steady-state fluorescence emission spectra were measured using a Photon Technology International MP-1 spectrometer and were corrected for detection system response. Excitation was provided by a 75 W xenon-arc lamp and single grating monochromator. Fluorescence was detected 90 degree to the excitation beam via a single grating monochromator and a R928 photomultiplier tube having S-20 spectral response operating in the single photon counting mode. The SPEST (in EtOH) sample was deoxygenated by purging the sample with argon for 30 minin the dark. The SP-PVDF-*co*-HFP mat was stretched flat and sandwiched between two quartz plates to perform the spectroscopic measurements. For the fluorescence measurements, the plates were aligned 45 degree with respect to the incident beam and the emission slit such that the excitation light was not reflected into the detector.

3. Results and discussion

3.1. Scanning electron microscopy

SEM images of PVDF-*co*-HFP and SP-PVDF-*co*-HFP ES fibers fabricated at different concentrations of PVDF-*co*-HFP in DMAc-acetone are shown in Fig. 2. For the SP-PVDF-*co*-HFP samples, the concentration of SPEST was kept constant at 1 wt% relative to PVDF-*co*-HFP. As shown in Fig. 2a, pure PVDF-*co*-HFP ES fibers fabricated using 10 wt% solution adopt a bead-on-string morphology; however, using higher concentrations (12 and 15 wt%) results in the formation of fibers (Fig. 2b and c), although the fiber diameters are not uniform. When SPEST (1 wt%) is added to the 10 wt% PVDF-*co*-HFP solution, the resulting ES fibers exhibit a more narrow distribution of diameters, Fig. 2d. In fact, more uniform diameters are observed for ES SP-PVDF-*co*-HFP fibers ($2.25 \pm 0.19\ \mu m$) than for pure ES PVDF-*co*-HFP fibers for all concentrations of PVDF-*co*-HFP tested. This phenomenon is thought to be attributed to an increase in solution conductivity upon addition of SPEST. For example, the conductivity of a 15 wt% solution of PVDF-*co*-HFP in DMAc-acetone was measured to be 0.89 μS/cm, whereas the addition of 1 wt% SPEST increased the conductivity to 1.17 μS/cm. In general, an increase in solution conductivity causes higher extensional stress on the electrospun jet due to the action of the external electrical field on the charged jet in addition to charge repulsion on the jet. The higher extensional stress suppresses the Rayleigh instability completely during the electrospinning process and leads to the formation of uniform fibers [68–72].

3.2. Fiber internal morphology

The internal fiber morphology of ES fibers was characterized by DSC, WAXD and FTIR. Pure PVDF-*co*-HFP copolymer is a semi-crystalline material, where the PVDF components are partially crystallized [73]. The wide angle X-ray (WX-ray) spectrum of PVDF-*co*-HFP solution-cast film, ES pure PVDF-*co*-HFP fibers and ES PVDF-*co*-HFP fibers containing 1 wt% SPEST are compared in Fig. 3. The WX-ray spectrum for pure PVDF-*co*-HFP ES fibers and SP-PVDF-*co*-HFP ES fibers are nearly identical, indicating that the addition of SPEST exerts no significant effect on the overall fiber internal morphology. All three samples show two strong peaks at $2\theta = 18.5°$ and 20.6°. The peak at $2\theta = 18.5°$ corresponds to 020 reflection of the α-phase having trans-gauche-trans-gauche′ (TGTG′) transformation while the peak at $2\theta = 20.6°$ corresponds to 200/100 reflections of the β-phase having all-trans (TTTT) conformation [73,74]. This result supports the co-existence of both the α-phase and β-phase in all the samples. However, the ratios of the peak heights ($2\theta = 18.5°$–20.6°) are 0.74 and 0.80 for the fiber samples and the film sample, respectively, which suggests that more β-phase is present within the fiber samples than within the film sample.

The FTIR spectra of pure PVDF-*co*-HFP ES fiber and solution-cast film are compared in Fig. 4. α-Phase-related bands (614, 765, 795 and 975 cm^{-1}), β-phase-related bands (840 and 1278 cm^{-1}) and

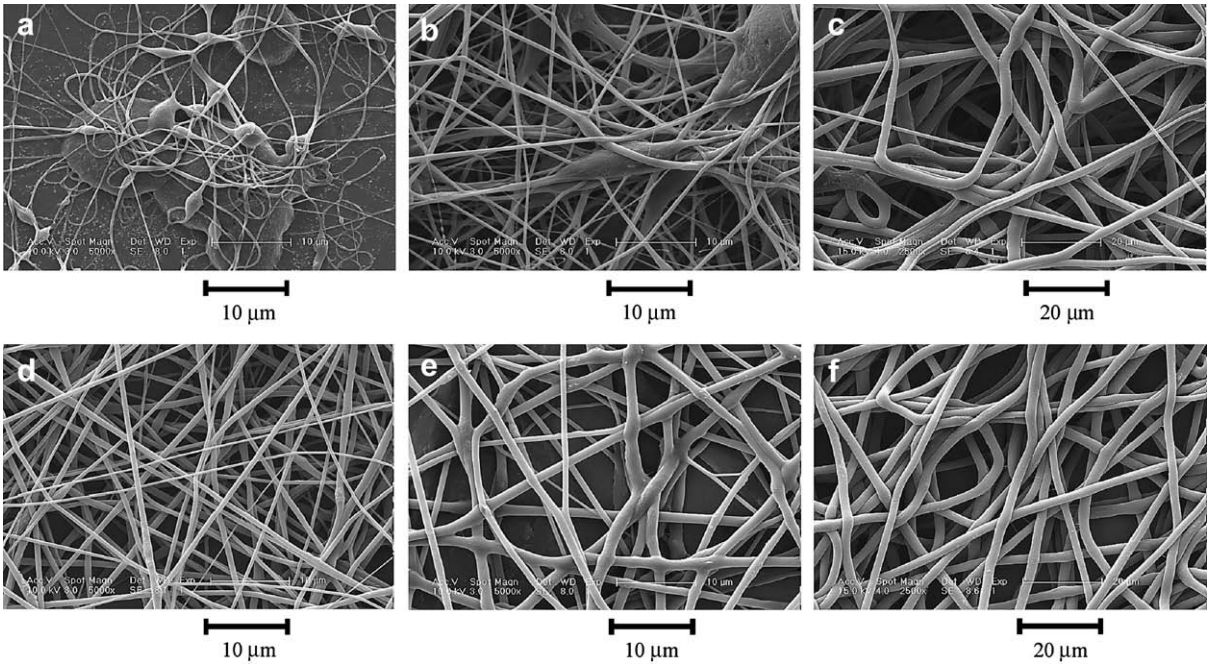

Fig. 2. SEM images of ES fibers of PVDF-*co*-HFP: (a) 10 wt%, (b) 12 wt%, (c) 15 wt% and ES fibers of SP-PVDF-*co*-HFP (containing 1 wt% SPEST): (d) 10 wt%, (e) 12 wt%, (f) 15 wt%.

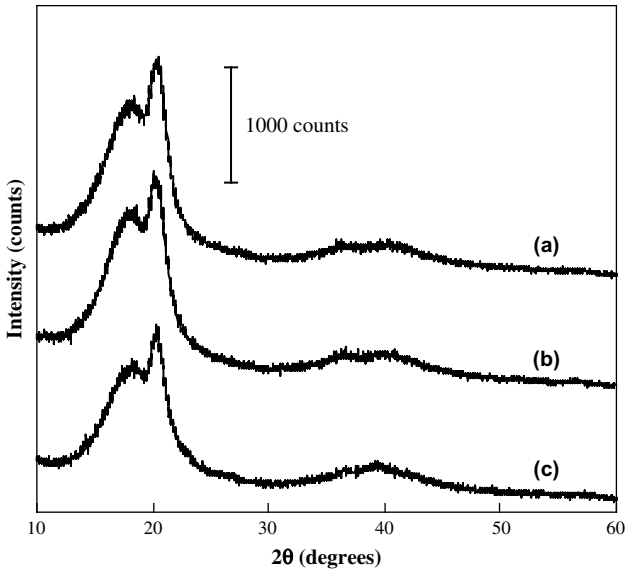

Fig. 3. Comparison of wide angle X-ray diffraction spectra of SP-PVDF-*co*-HFP fibers (a), ES PVDF-*co*-HFP fibers (b), and solution-cast film (c). The spectra have been offset on the *y*-axis to facilitate comparison and the scale bar indicates relative intensity.

γ-phase (TTTGTTTG′) bands at 1225 cm^{-1} are observed in both samples [75], indicating that all three phases of crystals are present in both samples. The relative intensity of the β-phase-related band (at 1278 cm^{-1}) was higher for the PVDF-*co*-HFP ES fibers than for the PVDF-*co*-HFP solution-cast film, however the relative intensity of the γ-phase-related band (at 1225 cm^{-1}) exhibited the opposite trend. Therefore, both X-ray and FTIR data show that the electrospinning process promotes the transition of α-phase and γ-phase crystals to β-phase crystals within ES fibers. The transition is thought to be due to the extensional stress applied on the liquid jet by electrostatic forces generated during the electrospinning process, which stretches the molecules and induces the conformational changes. These results are consistent with the conclusions for PVDF ES fibers reported previously by Gao et al. and Yee et al. [74,75].

3.3. Fiber surface morphology

The distribution of chemical components on the fiber surface was characterized by X-ray photoelectron spectroscopy (XPS). XPS experiments were performed on multiple samples of ES PVDF-*co*-HFP fibers with and without encapsulated spiropyran, where the presence of SPEST was confirmed by noting the change from colorless to red upon UV irradiation of those fiber samples. The XPS spectrum for ES PVDF-*co*-HFP fibers containing 1 wt% of SPEST is shown in Fig. 5, which is close to the XPS spectrum for pure ES PVDF-*co*-HFP fiber (Fig. 5, inset). The spectrum for the SP-PVDF-*co*-HFP shows three peaks that represent the F 1s (688 eV), the O 1s (529 eV) and the C 1s (281 eV) in the ratio 6.7:1.6:1. As shown in Fig. 5 for SP-PVDF-*co*-HFP, no peak was observed around 400 eV, which corresponds to the region characteristic of nitrogen (N 1s). The absence of this peak indicates that the spiropyran molecules are encapsulated towards the core of the fibers, or are embedded at least 5 nm beneath the fiber surface.

The lack of surface spiropyran can be explained in terms of both the low surface tension of the abundant fluorine-rich groups and the low glass transition temperature (T_g) of PVDF-*co*-HFP copolymers. The reported values for the surface tension of PVDF and poly(hexafluoropropylene) are 33.2 dyn/cm and 17.0 dyn/cm, respectively, at 20 °C [76]. Driven by the decrease in surface tension, most of the fluorine-rich groups readily migrate to the fiber surface during the electrospinning process. The T_g of PVDF-*co*-HFP copolymers is around −40 °C [73], which is well below the temperature at which the measurements are taken. Conceivably, the PVDF-*co*-HFP polymer chain in the amorphous phase could continue to reorient itself to allow fluorine migration towards the fiber surface after electrospinning until the spiropyran molecules are predominantly encapsulated within the PVDF-*co*-HFP fiber matrix. In this way, the fluorine-enriched fiber surface could function as a protective barrier for spiropyran molecules in adverse environments during various applications. Notably, spiropyran diffusion out of the fiber was not observed for a sample of SP-PVDF-*co*-HFP submerged in deionized water for 72 h.

The surface morphology of the ES fiber mats was characterized by contact angle (CA) measurements. The water contact angle on ES fiber mats is related to both the roughness of the fiber mats and the chemical components on the fiber surface. Photographs of water droplet profiles on samples of PVDF-*co*-HFP and SP-PVDF-*co*-HFP ES fibers are displayed in Fig. 6. The dynamic advancing water CA on the ES PVDF-*co*-HFP fiber mat, ES SP-PVDF-*co*-HFP fiber mat following UV irradiation ($\lambda = 365$ nm, 10 min) and ES SP-PVDF-*co*-HFP fiber mat following exposure to visible light ($\lambda > 520$ nm,

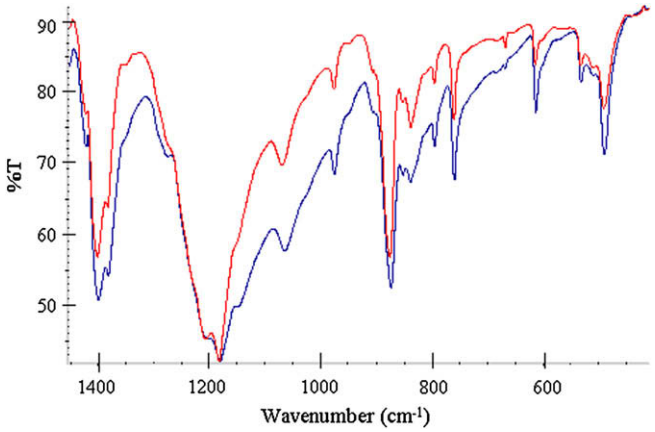

Fig. 4. FTIR spectra of PVDF-*co*-HFP ES fibers (blue) and PVDF-*co*-HFP solution-cast film (red).

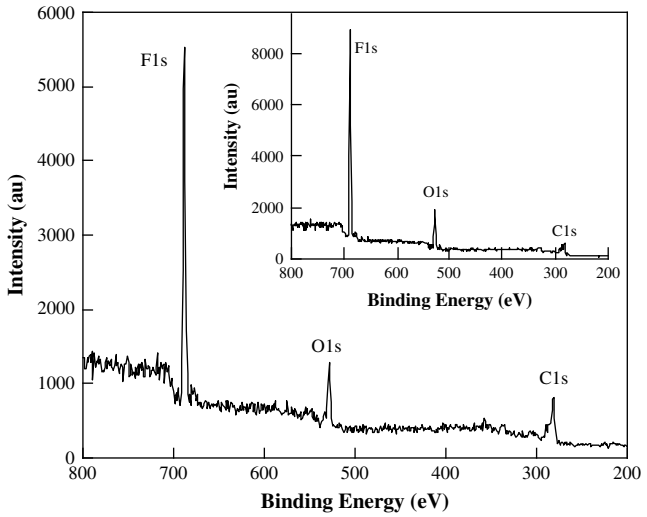

Fig. 5. XPS spectrum of SP-PVDF-*co*-HFP fibers. Inset shows XPS spectrum of pure PVDF-*co*-HFP fibers.

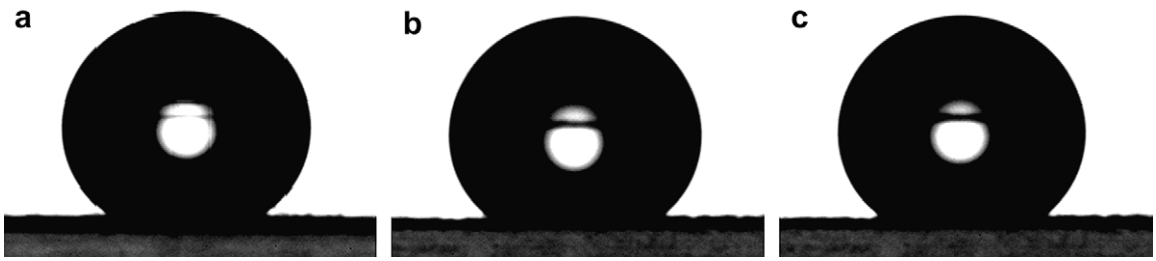

Fig. 6. Water contact angles: (a) ES fibers of PVDF-*co*-HFP, (b) ES fibers of SP-PVDF-*co*-HFP after UV irradiation for 10 min and (c) ES fibers of SP-PVDF-*co*-HFP after visible light irradiation for 10 min.

10 min) are $152^\circ \pm 1^\circ$, $146^\circ \pm 2^\circ$ and $143^\circ \pm 1^\circ$, respectively. The slight decrease in water CA for the SP-PVDF-co-HFP fiber mat relative to PVDF-co-HFP fiber mat is likely due to the decreased roughness in the former case that is caused by the more uniform diameter distribution of the SP fibers as was shown in the SEM images. There is no significant difference in CA for SP fiber mats following irradiation with UV or visible light. However, the pronounced photocoloration and decoloration confirm the efficient 'switching' of the spiropyran moiety within the fibers (Fig. 7). In all cases, the receding contact angle could not accurately be resolved, presumably due to the rough surface morphology of the fiber. Based on these observations, it is reasonable to suggest that the spiropyran moiety is not located on the surface, or near enough to the surface, to influence surface polarity to any significant extent, which is consistent with the XPS results.

3.4. Photochromic properties

The steady-state absorption spectra of SPEST in deoxygenated 100% ethanol (EtOH) and in PVDF-*co*-HFP are shown in Fig. 8. The absorption spectrum of SPEST in EtOH under dark conditions (Fig. 8, dotted black line) is characteristic of the SP (closed) form and exhibits absorption maxima at 338 nm and at several wavelengths <300nm. Following UV irradiation ($\lambda = 365$ nm, 1 min), a decrease in absorption in the UV region of the spectrum is accompanied by the formation of new absorption bands centered at 349 and 550 nm (Fig. 8, dashed black line). The bathochromic shift in absorption is due to the extended conjugation provided by the MC (open) form as compared to the SP form [77]. An absorption spectrum of the somewhat translucent SP-PVDF-*co*-HFP fibers was acquired by placing the ES fiber mat between two quartz plates and tightly focusing the incident beam of the spectrophotometer onto the sample. The dark (non-irradiated) sample was used as a background reference and the absorption spectrum shown in Fig. 8 (solid black line) was collected following exposure of the sample to UV irradiation ($\lambda = 365$ nm, 1 min). The absorption spectrum of the MC form of the SP-PVDF-*co*-HFP ES fiber sample closely resembles that of the MC form of SPEST in EtOH, with strong absorption in the 500–600 nm region. The small dip at the peak of the band is thought to be an artifact arising from the low amount of light transmitted through the sample in addition to scattering from the translucent material. Fig. 8 also presents the steady-state emission (fluorescence) spectra collected following 510 nm excitation of the MC form of SPEST in EtOH (dashed grey line) and in SP-PVDF-*co*-HFP (solid grey line). These spectra feature emission bands centered at 647 and 645 nm, respectively. No fluorescence was observed upon visible excitation of the SP form of SPEST in EtOH, which is consistent with previous reports [55].

Although the spectroscopic properties of SPEST in the ES fiber are closely similar to those observed in solution, the photochemical behavior exhibited by SPEST encapsulated as SP-PVDF-*co*-HFP varied from that seen in EtOH. A series of emission spectra acquired at 45 s intervals for SPEST (MC form) in EtOH ($\lambda_{ex} = 400$ nm) showed a decrease in emission intensity at 647 nm with no change in the shape of the emission band. This decrease in intensity can be attributed to both thermal and photochemical conversion of the fluorescent MC form to the non-emissive SP form, where the excitation beam is responsible for the photochemical transformation. When the same experiment was carried out with the SP-PVDF-*co*-HFP sample, the decay of fluorescence from the MC form monitored at *ca.* 640 nm was concomitant with a blue shift in this emission band and an increase in intensity at 468 and 482 nm, Fig. 9. These latter emission bands can be attributed to phosphorescence from the SP (closed form) triplet state (T1) [77]. Notably, the reverse reaction was also observed, *i.e.*, the SP to MC conversion, where 365 nm excitation of the SP form of SP-PVDF-*co*-HFP resulted in a decrease in emission at 468 and 482 nm and an increase in intensity in the 640 nm region.

The observation of phosphorescence from the SP-PVDF-*co*-HFP fiber on the time scale of the experiment suggests that the quantum yield of ring opening (SP–MC) in the ES fiber is significantly lower than for SPEST in EtOH. In other words, 400 nm excitation of the SP

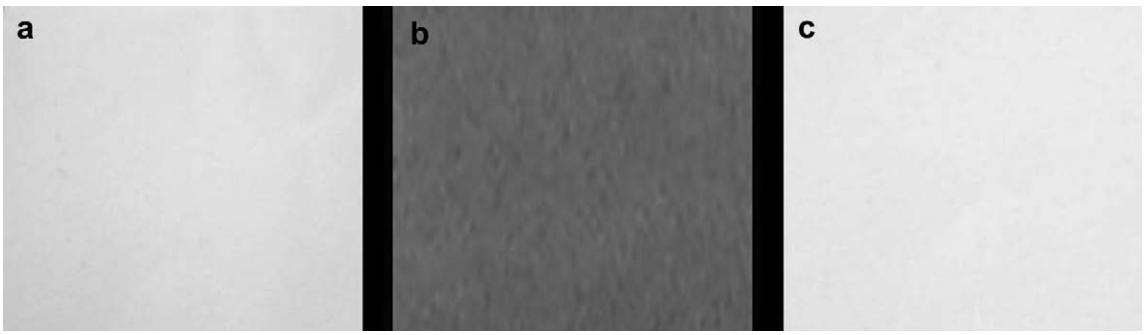

Fig. 7. Digital photographs of (SP-PVDF-*co*-HFP) following exposure to (a) no irradiation, (b) UV ($\lambda = 365$ nm, 10 min) and (c) visible light ($\lambda > 520$ nm, 10 min).

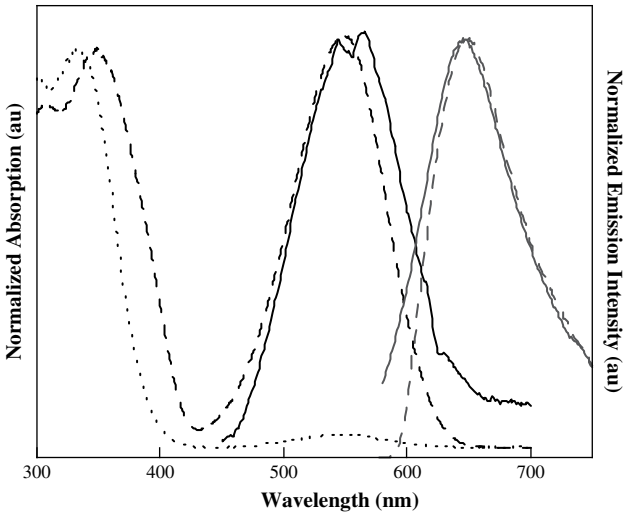

Fig. 8. Normalized absorption spectra of SPEST in deoxygenated 100% ethanol under the following conditions: dark (dotted black line) and following exposure to 365 nm irradiation for one minute (dashed black line). The solid black line represents the absorption spectrum of the SP-PVDF-*co*-HFP fiber mat acquired following exposure to UV irradiation for one minute (see text). The grey colored lines show the normalized emission spectra of SPEST in deoxygenated 100% ethanol following one minute of 365 nm irradiation (dashed grey line) and the SP-PVDF-*co*-HFP ES mat (solid grey line) following 2 min of 365 nm irradiation. In both cases, the excitation wavelength was 510 nm.

form of SPEST in EtOH results in a fast, efficient ring opening reaction and hence no tangible emission, whereas the less efficient ring opening process of the SP form in SP-PVDF-*co*-HFP gives rise to more observed emission from the spiropyran. Presumably, the matrix of the fibrous SP-PVDF-*co*-HFP mat imposes steric and/or electrostatic restrictions on SPEST that substantially retard the ring opening (and closing) processes. A similar effect has been observed for an ester-functionalized photomerocyanine incorporated within an organogel [78] nitrospiropyrans in zeolite Y [79] and room temperature ionic liquids [80]. This type of two-color emission that depends on the state of the photochrome in SP-PVDF-*co*-HFP could find applications in molecular switches or devices where two measurable outputs are desired.

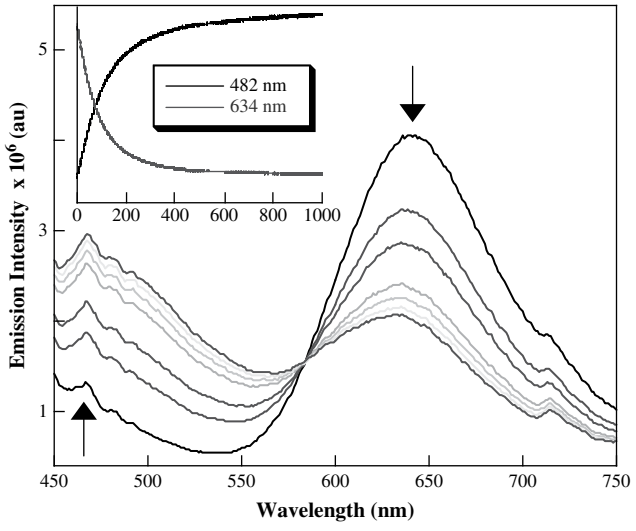

Fig. 9. Emission spectra obtained at 45 s intervals for SPEST-PVDF-*co*-HFP (MC form; after 5 min of UV irradiation) upon 400 nm excitation. Inset shows the kinetic traces corresponding to the change in emission intensity monitored at 482 nm (black line) and 634 nm (grey line).

4. Conclusion

Photochromic PVDF-*co*-HFP fibers were prepared by electrospinning a mixed solution of PVDF-*co*-HFP copolymer and spiropyran (SPEST, 1 wt%). Addition of SPEST to the solution facilitates the formation of uniform ES fibers due to the increased solution conductivity, which proceeds with preservation of fiber internal morphology. Migration of fluorine-rich groups onto the fiber surface, which is driven by lower surface tension and occurs during and/or after the electrospinning process, leads to the encapsulation of SPEST predominantly near the core of the fibers, as confirmed by both XPS and dynamic water CA measurements. The photochromic behavior of the spiropyran is preserved in the polymeric fibers as demonstrated by steady-state absorption and emission spectroscopy. Emission was observed from both the open and closed forms of SP-PVDF-*co*-HFP, due to the lower quantum yield of ring opening that results from the steric and/or electronic restrictions placed on the photochrome by the ES fiber.

Acknowledgments

S.A.V. gratefully acknowledges the INEST Postdoctoral Program (Philip Morris USA) for financial support. We thank Timothy Karcher of the LeRoy Eyring Center for Solid State Science (Arizona State University) for XPS surface analysis, and Vicki L. Baliga and Jeffrey Molnar (PMUSA) for SEM analysis. WAXD data for this publication was carried in the Center for Microanalysis of Materials, University of Illinois at Urbana-Champaign, which is partially supported by the U.S. Department of Energy under grant DEFG02-91ER45439. We thank Jacinta Conrad for providing the WAXD data.

References

[1] Dzenis Y. Science 2004;304:1917.
[2] McKee MG, Layman JM, Cashion MP, Long TE. Science 2006;311:353.
[3] Bognitzki M, Czado W, Frese T, Schaper A, Hellwig M, Steinhart M, et al. Adv Mater 2001;13:70.
[4] Ma Z, Kotaki M, Ramakrishna S. J Membr Sci 2005;265:115.
[5] Gopal R, Kaur S, Ma Z, Chan C, Ramakrishna S, Matsuura T. J Membr Sci 2006;281:581.
[6] Wang X, Fang D, Yoon K, Hsiao BS, Chu B. J Membr Sci 2006;278:261.
[7] Senecal KJ, Senecal AG, Pivarnik PE, Mello CM, Soares JW, Schreuder-Gibson HL. U.S. Patent. Appl.; 2006.
[8] Verreck G, Chun I, Rosenblatt J, Peeters J, Van Dijck A, Mensch J, et al. J Controlled Release 2003;92:349.
[9] Zeng J, Aigner A, Czubayko F, Kissel T, Wendorff JH, Greiner A. Biomacromolecules 2005;6:1484.
[10] Jiang H, Hu Y, Li Y, Zhao P, Zhu K, Chen W. J Controlled Release 2005;108:237.
[11] Xie J, Wang C-H. Pharm Res 2006;23:1817.
[12] Taepaiboon P, Rungsardthong U, Supaphol P. Nanotechnology 2006;17:2317.
[13] Ding B, Kim J, Fujimoto K, Shiratori S. Chem Sensors 2004;20:264.
[14] Wang X, Kim Y-G, Drew C, Ku B-C, Kumar J, Samuelson LA. Nano Lett 2004;4:331.
[15] Katarzyna S, Perena G, Sanford S. Sens Actuators, B 2005;108:585.
[16] Li D, Frey MW, Baeumner AJ. J Membr Sci 2006;279:354.
[17] Li M, Mondrinos MJ, Gandhi MR, Ko FK, Weiss AS, Lelkes PI. Biomaterials 2005;26:5999.
[18] Park KE, Jung SY, Lee SJ, Min B-M, Park WH. Int J Biol Macromol 2006;38:165.
[19] Gibson P, Schreuder-Gibson H, Rivin D. Colloids Surf A 2001;187–188:469.
[20] Huang C, Chen S, Reneker DH, Lai C, Hou H. Adv Mater 2006;18:668.
[21] Teo WE, Kotaki M, Mo XM, Ramakrishna S. Nanotechnology 2005;16:918.
[22] Teo WE, Ramakrishna S. Nanotechnology 2005;16:1878.
[23] Li D, Ouyang G, McCann JT, Xia Y. Nano Lett 2005;5:913.
[24] Chuangchote S, Supaphol P. J Nanosci Nanotechnol 2006;6:125.
[25] Kim GH, Kim WD. Appl Phys Lett 2006;88:233101.
[26] Jalili R, Morshed M, Abdolkarim S, Ravandi H. J Appl Polym Sci 2006;101:4350.
[27] Kakade M, Givens S, Chase B, Rabolt J. PMSE Prepr 2006;94:614.
[28] McCann JT, Chen JIL, Li D, Ye Z-G, Xia Y. Chem Phys Lett 2006;424:162.
[29] Deitzel JM, Kosik W, McKnight SH, Beck Tan NC, DeSimone JM, Crette S. Polymer 2002;43:1025.
[30] Ma M, Hill RM, Lowery JL, Fridrikh SV, Rutledge GC. Langmuir 2005;21:5549.
[31] Ma M, Krikorian V, Yu JH, Thomas EL, Rutledge GC. Nano Lett 2006;12:2969.
[32] Kalra V, Mendez S, Lee JH, Nguyen H, Marquez M, Joo YL. Adv Mater 2006;18:3299.

[33] Kalra V, Kakad PA, Mendez S, Ivannikov T, Kamperman M, Joo YL. Macromolecules 2006;39:5453.
[34] Wang M, Singh H, Hatton TA, Rutledge GC. Polymer 2004;45:5505.
[35] Li M, Guo Y, Wei Y, MacDiarmid AG, Lelkes PI. Biomaterials 2006;27:2705.
[36] Salalha W, Dror Y, Khalfin RL, Cohen Y, Yarin AL, Zussman E. Langmuir 2004;20:9852.
[37] Li D, Xia Y. Nano Lett 2003;3:555.
[38] Jin H-J, Fridrikh SV, Rutledge GC, Kaplan DL. Biomacromolecules 2002;3:1233.
[39] Wang M, Jin H-J, Kaplan DL, Rutledge GC. Macromolecules 2004;37:6856.
[40] Loscertales IG, Barrero A, Guerrero I, Cortijo R, Marquez M, Gañán-Calvo AM. Science 2002;295:1695.
[41] Yu JH, Fridrikh SV, Rutledge GC. Adv Mater 2004;16:1562.
[42] Sun Z, Zussman E, Yarin AL, Wendorff JH, Greiner A. Adv Mater 2003;15:1929.
[43] Wang M, Yu JH, Kaplan DL, Rutledge GC. Macromolecules 2006;39:1102.
[44] Song T, Zhang YH, Zhou TJ, Lim CT, Ramakrishna S, Liu B. Chem Phys Lett 2005; 415:317.
[45] Loscertales IG, Barrero A, Marquez M, Spretz R, Velarde-Ortiz R, Larsen G. J Am Chem Soc 2004;126:5376.
[46] Willner I, Rubin S, Cohen Y. J Am Chem Soc 1993;115:4937.
[47] Fujimoto K, Amano M, Horibe Y, Inouye M. Org Lett 2006;8:285.
[48] Higuchi A, Hamamura A, Shindo Y, Kitamura H, Yoon BO, Mori T, et al. Biomacromolecules 2004;5:1770.
[49] Edahiro J, Sumaru K, Tada Y, Ohi K, Takagi T, Kameda M, et al. Biomacromolecules 2005;6:970.
[50] Tomizaki K-Y, Mihara H. J Mater Chem 2005;15:2732.
[51] Bertelson RC. Photochromism, vol. 3. New York: Wiley-Interscience; 1971. p. 45–433.
[52] Durr H, Bouas-Laurent H. Photochromism: molecules and systems. New York: Elsevier; 1990.
[53] Galvin JM, Schuster GB. Supramol Sci 1998;5:89.
[54] Rosario R, Gust D, Hayes M, Jahnke F, Springer J, Garcia AA. Langmuir 2002;18:8062.
[55] Rosario R, Gust D, Hayes M, Springer J, Garcia AA. Langmuir 2003;19:8801.
[56] Rosario R, Gust D, Garcia AA, Hayes M, Taraci JL, Clement T, et al. J Phys Chem B 2004;108:12640.
[57] Mele E, Pisignano D, Varda M, Farsari M, Filippidis G, Fotakis C, et al. Appl Phys Lett 2006;88:203124.
[58] Ipe BI, Mahima S, Thomas KG. J Am Chem Soc 2003;125:7174.
[59] Zhu L, Zhu M-Q, Hurst JK, Li ADQ. J Am Chem Soc 2005;127:8968.
[60] Khairutdinov RF, Hurst JK. Langmuir 2004;20:1781.
[61] Nayak A, Liu H, Belfort G. Angew Chem Int Ed 2006;45:4094.
[62] Wang G, Bohaty AK, Zharov I, White HS. J Am Chem Soc 2006;128:13553.
[63] Vlassiouk I, Park C-D, Vail SA, Gust D, Smirnov S. Nano Lett 2006;6:1013.
[64] Maurer MK, Lednev IK, Asher SA. Adv Funct Mater 2005;15:1401.
[65] Bell NS, Piech M. Langmuir 2006;22:1420.
[66] Garcia A, Marquez M, Cai T, Rosario R, Hu Z, Gust D, et al. Langmuir 2007;23:224.
[67] Yang D, et al. Langmuir 2007;23:10864.
[68] Shin YM, Hohman MM, Brenner MP, Rutledge GC. Polymer 2001;42:9955.
[69] Shin YM, Hohman MM, Brenner MP, Rutledge GC. Appl Phys Lett 2001;78:1149.
[70] Yarin AL, Koombhongse SJ, Reneker DH. J Appl Phys 2001;89:3018.
[71] Wang M, Hsieh AJ, Rutledge GC. Polymer 2005;46:3407.
[72] Yu JH, Fridrikh SV, Rutledge GC. Polymer 2006;47:4789.
[73] Abbrent S, Plestil J, Hlavata D, Lindgren J, Tegenfeldt J, Wendsjo A. Polymer 2001;42:1407.
[74] Gao K, Hu X, Dai C, Yi T. Mater Sci Eng B 2006;131:100.
[75] Yess WA, Kotaki M, Liu Y, Lu X. Polymer 2007;48:512.
[76] Brandrup J, Immergut EH. Polymer handbook, vol. 31. New York: Wiley; 1998. 4th ed.
[77] Holm AK, Mohammed OF, Rini M, Mukhtar E, Nibbering ETJ, Fidder H. J Phys Chem A 2005;109:8962.
[78] Shumburo A, Biewer MC. Chem Mater 2002;14:3745.
[79] Schomburg C, Wark M, Rohlfing Y, Schulz-Ekloff G, Wöhrle D. J Mater Chem 2001;11:2014.
[80] Zhang S, Zhang Q, Ye B, Li X, Zhang X, Deng Y. J Phys Chem B 2009;113:6012.